# Phased Array Beam Fields of Nonlinear Rayleigh Surface Waves *

Shu-Zeng Zhang(张书增)[1], Xiong-Bing Li(李雄兵)[1], Hyunjo Jeong[2]**

[1]School of Traffic and Transportation Engineering, Central South University, Changsha 410075
[2]Division of Mechanical and Automotive Engineering, Wonkwang University, Iksan 570-749, Korea

(Received 2 April 2016)

*This study concerns calculation of phased array beam fields of the nonlinear Rayleigh surface waves based on the integral solutions for a nonparaxial wave equation. Since the parabolic approximation model for describing the nonlinear Rayleigh waves has certain limitations in modeling the sound beam fields of phased arrays, a more general model equation and integral forms of quasilinear solutions are introduced. Some features of steered and focused beam fields radiated from a linear phased array of the second harmonic Rayleigh wave are presented.*

PACS: 43.25.Fe, 43.25.Zx, 43.38.Hz DOI: 10.1088/0256-307X/33/7/074302

Acoustic phased array has become a noninvasive device featuring the large acoustic energy, high signal-to-noise ratio and high azimuth resolution of acoustic sound beam.[1] It is also convenient to simultaneously generate dynamic focusing and steering beams, and this flexibility can make ultrasonic inspections rapid and cost-effective.[2] In addition, phased array has been introduced to nonlinear acoustic applications, such as harmonic imaging in medical inspection,[3] defect detection in nondestructive evaluation,[4] and underwater communications.[5] Recently, the acoustic phased array technique has been extended to the Rayleigh waves, and a linear array of the Rayleigh wave transducers was also developed.[6,7] More recently, the nonlinear Rayleigh waves have been successfully applied to characterize microstructural changes induced by thermal, fatigue, or radiation damage.[8,9] The existing phased array technique combined with features of the nonlinear Rayleigh waves will better facilitate detection and localization of micro defects and material damages. It is necessary to predict the Rayleigh wave beam fields emitted from acoustic phased array to design a phased array system and to extract quantitative information from measurements.[6,10] A parabolic model equation for describing the nonlinear Rayleigh waves has been widely used to simulate the Rayleigh beam fields radiated from a line source.[11] However, the parabolic wave equation is not applicable to the regions very close to the source or far away from the acoustic axis, and causes difficulties in simulating focused or steered beam fields of phased array transducers. The purpose of this work is to model the nonlinear Rayleigh beam fields radiating from a linear phased array transducer with a nonparaxial solution to the nonlinear Rayleigh wave equation. Integral solutions for a quasilinear system of equations are obtained, and some new features on the phased array beam fields of the second harmonic Rayleigh wave are presented.

We consider a Rayleigh wave beam in an isotropic solid that occupies the half-space $z \leq 0$, and the nominal direction of propagation is along the $x$-axis, as depicted in Fig. 1. The characteristic parameters of the beam are the line source whose half-length is $a$, fundamental angular frequency $\omega_{\rm r}$, and the corresponding wave number $k_{\rm r} = \omega_{\rm r}/c_{\rm r}$, where $c_{\rm r}$ is the Rayleigh sound speed. The line source applied on the solid sample surface may generate not only the Rayleigh surface waves but also other waves such as bulk longitudinal and shear waves. In this work only the Rayleigh waves are considered and all other waves are ignored. We describe the Rayleigh waves in terms of only the $x$ and $z$ components of the particle velocity as[11]

$$v_x(x,y,z,t) = \frac{1}{2}\sum_{n=-\infty}^{\infty} u_{xn}(z) v_n(x,y) \cdot \exp(in(k_{\rm r}x - \omega_{\rm r}t)), \quad (1)$$

$$v_z(x,y,z,t) = \frac{1}{2}\sum_{n=-\infty}^{\infty} u_{zn}(z) v_n(x,y) \cdot \exp(in(k_{\rm r}x - \omega_{\rm r}t)), \quad (2)$$

where $v_n(x,y)$ is the $n$th order harmonic Rayleigh wave velocity beams. The depth dependences $u_{xn}$ and $u_{zn}$ in the solid are defined as

$$u_{xn}(z) = i(\mathrm{sgn}n)[\xi_{\rm t}\exp(|n|\xi_{\rm t}k_{\rm r}z) + \eta\exp(|n|\xi_{\rm l}k_{\rm r}z)], \quad (3)$$

$$u_{zn}(z) = \exp(|n|\xi_{\rm t}k_{\rm r}z) + \xi_{\rm l}\eta\exp(|n|\xi_{\rm l}k_{\rm r}z), \quad (4)$$

where $\xi_{\rm t} = (1-\xi^2)^{1/2}$, $\xi_{\rm l} = (1-\xi^2 c_{\rm t}^2/c_{\rm l}^2)^{1/2}$, $\eta = -2(1-\xi^2)^{1/2}/(2-\xi^2)$, $\xi = c_{\rm r}/c_{\rm t}$, and $c_{\rm t}$ and $c_{\rm l}$ are the phase speeds of shear wave and longitudinal wave, respectively. In a previous study,[11] diffraction effects in the nonlinear Rayleigh wave beams were taken into account within the parabolic approximation. The parabolic approximation is known to be valid for acoustic sources which are many wavelengths across and for field points that are not too close to the source or too far off axis. Here the model equation for the nonlinear Rayleigh waves with the parabolic approximation is modified to account for diffraction effects in a more general and accurate way. When the parabolic approximation is removed, the general

*Supported by the National Natural Science Foundation of China under Grant Nos 61271356 and 51575541, the National Research Foundation of Korea under Grant Nos 2013-M2A2A9043241 and 2013-R1A2A2A01016042, and the Hunan Provincial Innovation Foundation For Postgraduate under Grant No CX2016B046.

**Corresponding author. Email: hjjeong@wku.ac.kr

© 2016 Chinese Physical Society and IOP Publishing Ltd

spectral equation describing the propagation of the nonlinear Rayleigh wave beam is given by[12]

$$\frac{\partial^2 v_n}{\partial x^2}+\frac{\partial^2 v_n}{\partial y^2}+n^2k_{\rm r}^2v_n+2nik_{\rm r}\alpha_n v_n = \frac{2n^3k_{\rm r}}{v_0\bar{x}}\Big(2\sum_{m=n+1}^{\infty}R_{m,n-m}v_m v_{m-n}^* - \sum_{m=1}^{n-1}R_{m,n-m}v_m v_{n-m}\Big), \quad (5)$$

where $v_n^* = v_{-n}$, $\alpha_n$ is the attenuation coefficient at frequency $n\omega_{\rm r}$, $\bar{x} = 2\zeta\rho c_{\rm r}^3/\mu k v_0$ is a characteristic length scale, $\rho$ is the density of the material, $\mu$ is the shear modulus, $v_0$ characterizes the velocity amplitude at the source, $\xi = \xi_{\rm t}+\xi_{\rm t}^{-1}+\eta^2(\xi_{\rm l}+\xi_{\rm l}^{-1})+4\eta$, and the matrix $R_{ml}$ is defined in Ref. [13].

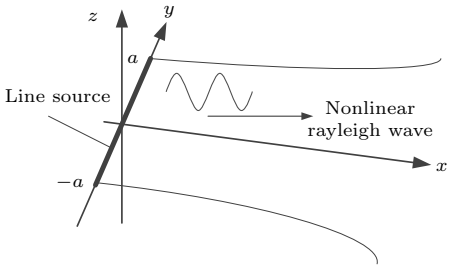


**Fig. 1.** Schematic diagram of the geometry of uniform line source and coordinate systems.

The solutions can be written in the time-harmonic form as

$$v_n(x,y) = |v_n(x,y)|\exp(-in\omega_{\rm r}t). \quad (6)$$

The line source condition at $x=0$ is defined as

$$v_1'(0,y) = w(y), \quad (7)$$
$$v_n'(0,y) = 0, \quad n>1. \quad (8)$$

It is thus assumed that the source does not radiate at harmonic frequencies, which suggests that harmonic waves are all generated by the propagating fundamental wave due to material nonlinearity.

In solid media, harmonic wave amplitudes are usually two or three orders of magnitude smaller than the fundamental wave amplitude. Thus it is reasonable to calculate the fundamental and second harmonic sound beams from Eq. (5) based on the quasilinear theory, $v = v_1+v_2$, where $|v_2(x,y)| \ll |v_1(x,y)|$ is assumed. With this assumption, Eq. (5) yields two governing wave equations for the fundamental and second harmonic components,

$$\frac{\partial^2 v_1}{\partial x^2}+\frac{\partial^2 v_1}{\partial y^2}+k_{\rm r}^2v_1+2ik_{\rm r}\alpha_1 v_1 = 0, \quad (9)$$
$$\frac{\partial^2 v_2}{\partial x^2}+\frac{\partial^2 v_2}{\partial y^2}+4k_{\rm r}^2v_2+4ik_{\rm r}\alpha_2 v_2 = -\frac{2\beta_{\rm r}k_{\rm r}^2}{c_{\rm r}}v_1^2, \quad (10)$$

where $\beta_{\rm r}$ is the nonlinearity parameter of the Rayleigh wave.[11]

We define Green's functions $G_n(r|r')$ here, at frequency $n\omega$, as the solution to the following inhomogeneous equation

$$\frac{\partial^2 G_n}{\partial x^2}+\frac{\partial^2 G_n}{\partial y^2}+(k_n')^2G_n = -\delta(\boldsymbol{r}-\boldsymbol{r}'), \quad (11)$$

where $k_n' = \sqrt{n^2k_{\rm r}^2+2nik_{\rm r}\alpha_n} \approx nk_{\rm r}+i\alpha_n$, and a two-dimensional Dirac delta function $\delta(\boldsymbol{r}-\boldsymbol{r}')$ is used. The Green's functions can be solved as[14]

$$G_n(r'|r) = \frac{-i}{4}\sqrt{\frac{2i}{nk_{\rm r}\pi r}}\exp(ink_{\rm r}r-\alpha_n r), \quad (12)$$

where $r = \sqrt{(x-x')^2+(y-y')^2}$ is the distance from the target point to the source position.

The integral solutions to Eqs. (9) and (10) can be constructed with Green's functions,

$$v_1(x,y) = -2ik_{\rm r}\int_{-a}^{a}w(y')G_1(r'|r)dy', \quad (13)$$
$$v_2(x,y) = -\frac{2\beta_{\rm r}k_{\rm r}^2}{c_{\rm r}}\int_0^x\int_{-\infty}^{+\infty}v_1^2(x',y')G_2(r'|r)dy'dx'. \quad (14)$$

Now, the nonparaxial solution to the nonlinear Rayleigh wave equation and the integral solutions for fundamental and second harmonic waves based on the quasilinear theory have been obtained. For comparison, the integral solutions for the parabolic wave equation[11] are given by

$$v_1(x,y) = \int_{-a}^{a}w(y')G_1(x,y|0,y')dy', \quad (15)$$
$$v_2(x,y) = -\frac{\beta_{\rm r}k_{\rm r}}{2c_{\rm r}}\int_0^x\int_{-\infty}^{+\infty}v_1^2(x',y')\cdot G_2(x,y|x',y')dy'dx' \quad (16)$$

with Green's function

$$G_n(x,y|x',y') = \sqrt{\frac{nk_{\rm r}}{i2\pi(x-x')}}\exp\Big(\frac{ink_0(y-y')^2}{2(x-x')} - \alpha_n(x-x')\Big). \quad (17)$$

A linear phased array radiating Rayleigh waves consists of single element sources, and each element source is approximated as an assembly of an infinitely large number of simple line sources arranged in the width direction. The array of elements can be steered and focused by applying an appropriate set of delays, called a delay law, to the elements.[2] When the sound beam behaviors are analyzed, we usually consider the static sound fields. Therefore, the phase term $\exp(ik_{\rm r}\Delta d)$, where $\Delta d$ is the distance difference and $k_{\rm r}\Delta d$ denotes the phase difference, for each element will be introduced for modeling the sound fields. Consider an array of $N$ elements radiating into a solid to produce a sound beam with steering angle of $\theta$ degrees and focusing distance of $F$ in units of m, as shown in

Fig. 2. The distance differences can be calculated as follows:

$$\Delta d_n = F\left[1+\left(\frac{\bar{N}d}{F}\right)^2+\frac{2\bar{N}d}{F}\sin\theta\right]^{1/2}-F\left[1+\left(\frac{(n-\bar{N})d}{F}\right)^2+\frac{2(n-\bar{N})d}{F}\sin\theta\right]^{1/2}, \quad (18)$$

where $\Delta d_n$ is the calculated distance difference for element $n = 0, 1, \ldots, N-1$, $\bar{N} = (N-1)/2$, and $d$ is the center-to-center spacing between elements. Beam steering and focusing can be achieved with these phase delays.

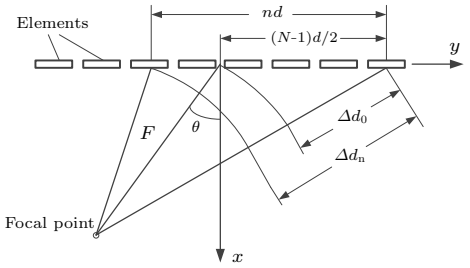


**Fig. 2.** Geometrical parameters for steering and focusing of a linear phased array.

The element width and gap between two elements in the phased array will affect the focused and steered beams. It has been proved that by appropriately changing the phases of broadly generated wave fields of small elements (less than one wavelength) one can easily adjust their combined effect to steer and focus the overall sound beam of the array.[2] In addition, it is found that the inter-element spacing should be less than half the wavelength to avoid grating lobes.[15] Thus element width and gap should be well chosen when the phased array is designed. In this work, a 48-element phased array will be used for simulating steered and focused beam fields. The fundamental frequency used is 1 MHz. The element size is 1.2 mm, and the center-to-center distance is 1.5 mm. The phased array radiates the Rayleigh waves into aluminum in which $c_r = 2940\,\mathrm{m/s}$, $c_s = 3170\,\mathrm{m/s}$ and $c_l = 6350\,\mathrm{m/s}$. The nonlinearity parameter used is $\beta_r = 0.22$.[16] The attenuation effects are ignored. Each element source is assumed to have the uniform velocity distribution with $w(0, y) = 1\,\mathrm{m/s}$. The particle velocity used in Eqs. (13)–(16) is converted to the particle displacement by using the relationship $v_n = -i\omega u_n$, $n = 1$ and 2. A transition range of the array is denoted by $Z_{TR} = D^2/4\lambda$, where $D$ is the overall dimension of the array, and $\lambda$ is the wavelength of the acoustic medium,[15] which is used to divide the near and far fields of a phased array transducer. The focal distance $F$ is set to be 0.15 m, which is within the transition range $Z_{TR} = 0.4\,\mathrm{m}$, thus focusing can be employed to increase the measurement resolution. Various steering angles (0°, 15°, 30° and 45°) are used, and phase delays for each element are introduced to achieve such behaviors. The nonparaxial results will be compared with the paraxial results.

Figure 3 represents the 2D displacement patterns of the fundamental Rayleigh waves for $\theta = 0°$, 15°, 30°, and 45° when the focal distance is fixed at $F = 0.15\,\mathrm{m}$. Figures 4 and 5 show the displacement distributions along the steering axis and along the cross axis, respectively, passing through the maximum amplitude of displacement profile.

It can be seen from Fig. 4 that the paraxial approximation does not recover the prescribed source amplitude at $x = 0$, and the predicted displacements are not valid for a small region close to the source. It is also noticed from Fig. 5 that the paraxial approximation causes abnormal displacements in the far transverse region. This happens due to the fact that $1/\sqrt{r}$ in Green's function is replaced by $1/\sqrt{x}$ in the paraxial approximation. It was also proved that the paraxial approximation loses accuracy when $y \gg x$.[17]

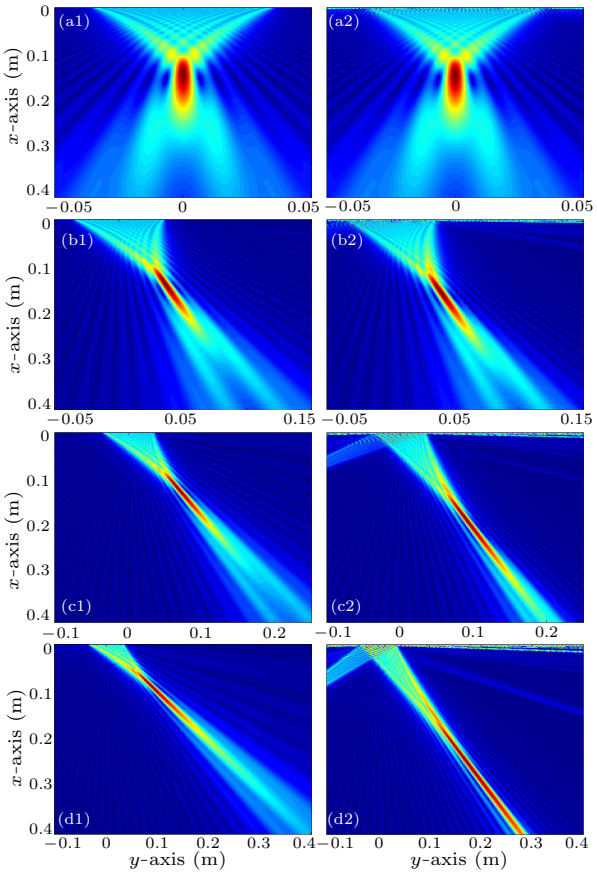


**Fig. 3.** The 2D displacement patterns of fundamental Rayleigh waves with the steering angles of (a) $\theta = 0°$, (b) $\theta = 15°$, (c) $\theta = 30°$, and (d) $\theta = 45°$, and $F = 0.15\,\mathrm{m}$. The left panel is the nonparaxial solution, while the right panel is the paraxial solution.

Another thing to note is the occurrence of grating lobes with the paraxial approximation in Figs. 3(c2) and 3(d2). The grating lobes are related to steering angles and ratio of wavelength and center-to-center distance of elements.[18] These unwanted grating lobes do not appear in the nonparaxial solutions.

Simulation results with the nonparaxial solutions (NPS) are compared with those with the paraxial solutions (PS). When the steering angle is 0°, both results show no deviation, as can be seen in Figs. 4(a) and 5(a). As the specified steering angle increases, however, deviation of the steered angle by the parax-

ial solution increases in Figs. 5(b)–5(d). Quantitative comparisons of steering angles are listed in Table 1. The steering angles predicted by NPS agree with the specified angles within ±0.5°. These results indicate the correct steering capability of NPS. However, PS causes huge errors in predicting the steered beams, for instance, as large as 15% smaller steering angle when the specified angle is $\theta = 45°$.

**Table 1.** Predicted steering angles by different methods.

| Specified angle (deg) | 0 | 15 | 30 | 45 |
|---|---|---|---|---|
| Fundamental, NPS (mm) | 0 | 15 | 29.8 | 44.8 |
| Fundamental, PS (mm) | 0 | 14.2 | 26.5 | 38 |
| 2nd harmonic, NPS (mm) | 0 | 15 | 29.7 | 44.5 |
| 2nd harmonic, PS (mm) | 0 | 13.9 | 26 | 36.5 |

**Table 2.** Predicted focal distances by different methods.

| Specified angle (deg) | 0 | 15 | 30 | 45 |
|---|---|---|---|---|
| Fundamental, NPS (mm) | 141 | 138 | 135 | 127 |
| Fundamental, PS (mm) | 142 | 160 | 202 | 290 |
| 2nd harmonic, NPS (mm) | 153 | 155 | 157 | 161 |
| 2nd harmonic, PS (mm) | 153 | 181 | 228 | 340 |

**Table 3.** Predicted focal spot sizes of the Rayleigh sound beams.

| Specified angle (deg) | 0 | 15 | 30 | 45 |
|---|---|---|---|---|
| Fundamental, NPS (mm) | 8.5 | 8.8 | 9.4 | 10 |
| 2nd harmonic, NPS (mm) | 5 | 5.6 | 6.2 | 6.8 |

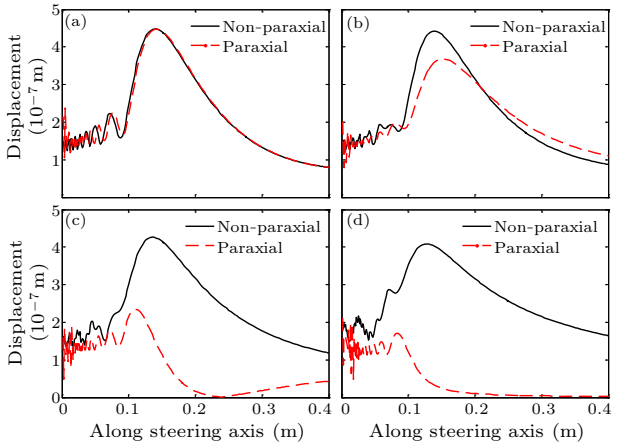


**Fig. 4.** Fundamental Rayleigh beam displacements calculated along the actual steering axis: (a) $\theta = 0°$, (b) $\theta = 15°$, (c) $\theta = 30°$, and (d) $\theta = 45°$.

The most noticeable difference between the two solutions is the focusing behavior of steering beams. The results are shown in Fig. 4, and quantitative comparisons between NPS and PS are summarized in Table 2, where the focal distance in each case is predicted along the actual steering axis. The maximum displacement predicted by NPS does not always occur at the original focal point, as can be seen in Table 2. The deviation of the actual focal point from the specified focal distance increases with increasing the steering angle. This is due to the geometric diffusion of sound waves that tends to bring the point of maximum beam intensity nearer to the transducer in the steering direction. The paraxial solution, on the contrary, causes serious problems such as grating lobe and false beam focusing when the steering angle is greater than $\theta = 30°$ (see Table 2). PS predicts the focal distances of the steered fundamental Rayleigh beams at much longer distances than the specified. In addition, the displacement amplitudes at the focal points obtained with PS are much smaller than those with NPS.

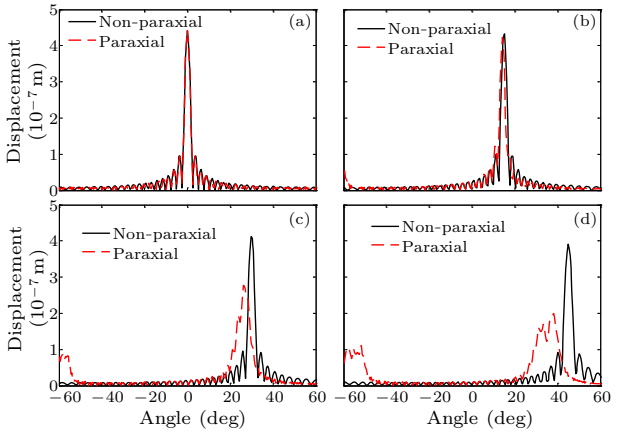


**Fig. 5.** Fundamental Rayleigh beam displacements calculated along the cross axis at $F = 0.15$ m: (a) $\theta = 0°$, (b) $\theta = 15°$, (c) $\theta = 30°$, and (d) $\theta = 45°$.

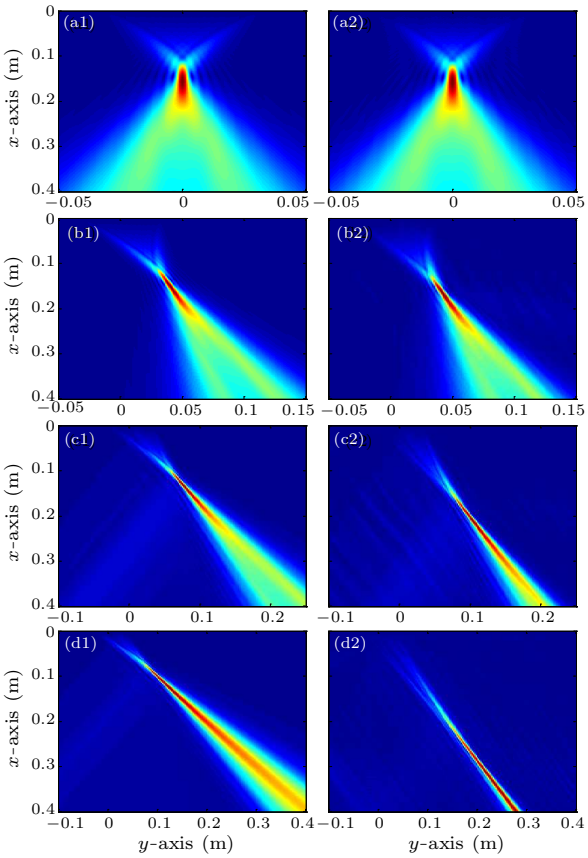


**Fig. 6.** The 2D displacement patterns of the second harmonic Rayleigh waves corresponding to the fundamental wave cases. The left panel is the nonparaxial solution, while the right panel is the paraxial solution.

Focused and steered fundamental waves are obtained by changing the element phases. With these waves working as the sound sources for generating second harmonic waves, the focused and steered nonlinear wave beams can be calculated. Figure 6 represents the 2D displacement patterns of the second harmonic Rayleigh sound beams. Figures 7 and 8 show the displacement distribution along the steering axis

and along the cross axis, respectively, passing through the maximum amplitude of the displacement profile. Actual steering angles and focal distances are listed in Tables 1 and 2. The second harmonic beam is produced by the forcing of the fundamental wave, and thus similar behavior can be observed for steering angles predicted by NPS, as seen in Table 1.

The most noticeable difference is observed in focusing behavior of second harmonic beams, as seen in Table 2. The fundamental beam focuses at a shorter distance than the initially specified length, and this focal distance decreases as the steering angle increases. However, the second harmonic beam shows a focal distance longer than the predicted fundamental case, and it is also found that this focal distance increases with the steering angle. One of the reasons is that the fundamental wave acts as the sound source for the second harmonic, and the near field effects in the second harmonic field extend further from the source rather than those in the fundamental field.

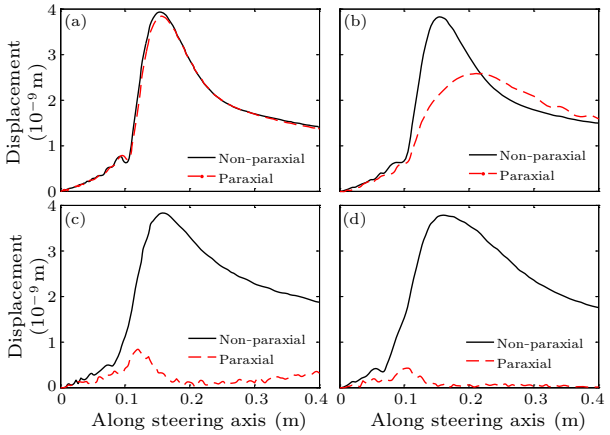


**Fig. 7.** The second harmonic Rayleigh beam displacements calculated along the actual steering axis: (a) $\theta = 0°$, (b) $\theta = 15°$, and (c) $\theta = 30°$, and (d) $\theta = 45°$.

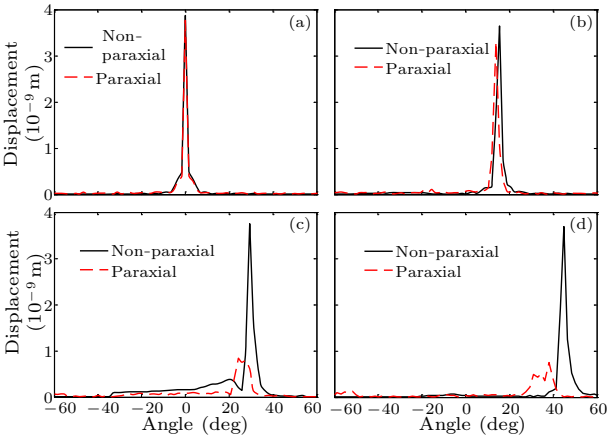


**Fig. 8.** The second harmonic Rayleigh beam displacements calculated along the cross axis at $F = 0.15$ m: (a) $\theta = 0°$, (b) $\theta = 15°$, (c) $\theta = 30°$, and (d) $\theta = 45°$.

The spatial focusing property of phased array is important in various applications including nondestructive testing, thus we need to examine the focal spot size of the focused beam. In a homogeneous medium, it is known that the phase array signal will focus in a region around the specified focal point with spatial width (or focal spot size) of order $d = \lambda F/D$. The estimated focal spot size of the fundamental phased array beam is about 6.5 mm. Table 3 summarizes the focal spot sizes of the fundamental and second harmonic beams measured at 6 dB from Figs. 3 and 6. The measured focal spot sizes of fundamental beams are slightly larger than the estimated value, and this difference becomes larger with increasing the steering angle. The measured focal spot size of the second harmonic beam is, as expected, narrower than the fundamental beam, which means that the focused second harmonic beam will provide enhanced spatial resolution.

In summary, the fundamental and second harmonic Rayleigh wave beams radiating from a linear phased array with uniform line source have been studied by using a nonparaxial wave equation. The nonparaxial solutions could predict the more reasonable steering and focusing behavior for both fundamental and second harmonic Rayleigh beams. The simulation results show that the predicted fundamental beams are focused at distances shorter than the specified focal distances, and the deviation of the actual focal distance from the specified distance increases with the steering angle. However, the maximum amplitudes of the focused second harmonic beams occur at distances longer than the fundamental focal distances. It is also found that the focal distance of the second harmonic increases with the steering angle. The focused second harmonic beams show the beam widths narrower than the focused fundamental beams. These simulation results can be used as guidelines for designing phased array transducers of the nonlinear Rayleigh waves. Future experimental work should verify the simulation results presented in this study.

## References

[1] Fujisawa K 2015 *Appl. Acoust.* **95** 57
[2] Schmerr L W 2014 *Fundamentals of Ultrasonic Phased Arrays* (New York: Springer)
[3] Bouakaz A et al 2003 *IEEE Trans. Ultrason. Ferroelectr. Freq. Control* **50** 730
[4] Potter J N et al 2014 *Phys. Rev. Lett.* **113** 144301
[5] Karsten W et al 2012 *ECUA 2012 11th European Conference on Underwater Acoustic* (Edinburgh, Scotland 2–6 July 2012) **17** 1
[6] Deutsch W A K et al 1997 *Res. Nondestr. Eval.* **9** 81
[7] Deutsch W A K et al 1999 *IEEE Trans. Ultrason. Ferroelectr. Freq. Control* **46** 333
[8] Kim G et al 2014 *NDTE Int.* **67** 64
[9] Thiele S et al 2014 *Ultrasonics* **54** 1470
[10] Ourak M et al 1999 *Review of Progress in Quantitative Nondestructive Evaluation* **18A** p 119
[11] Shull D J et al 1995 *J. Acoust. Soc. Am.* **97** 2216
[12] Zhang S et al 2016 *Mod. Phys. Lett.* B **30** 1650096
[13] Zabolotskaya E A 1992 *J. Acoust. Soc. Am.* **91** 2569
[14] Watanabe K 2014 *Integral Transform Techniques for Green's Function* (New York: Springer)
[15] Azar L et al 2000 *NDTE Int.* **33** 189
[16] Hurley D C 1999 *J. Acoust. Soc. Am.* **106** 1782
[17] Cervenka M and Bednarik M 2013 *J. Acoust. Soc. Am.* **134** 933
[18] Wooh S C and Shi Y 1998 *Ultrasonics* **36** 737